



Simulation of inclined dense jets in stagnant environments: an LES and experimental study

Hessam Tofighian¹ · Abdolreza Aghajanpour² · Ozeair Abessi² ·
Mohammadmehdi Ramezani²

Received: 2 October 2021 / Accepted: 26 June 2022 / Published online: 19 July 2022
© The Author(s), under exclusive licence to Springer Nature B.V. 2022

Abstract

Inclined dense jets are commonly used to mitigate the environmental impacts of brine discharge in coastal desalination plants. Numerous studies have been performed to numerically simulate the sophisticated structures of the flow within this process. However, numerical prediction of the process is still a challenge. The present paper performs a comprehensive numerical study using the large eddy simulation (LES) approach on inclined dense jets oriented at angles 15°, 30°, 45°, 60°, and 75°, with a particular emphasis on the near-wall region, where the most complicated structures of the flow occur. The objective is to evaluate the capability of the LES approach to replicate the mixing processes of the brine jets. Besides numerical simulations, a series of experiments using the planar laser-induced fluorescence technique is carried out to compare each numerical simulation with its experimental correspondence. Both numerical and experimental results are presented in comparative figures compared to previous experimental data. The comparisons indicated that the LES model could reasonably predict the geometrical and mixing characteristics of inclined dense jets; however, the flow features are still underestimated by up to 25%. Moreover, the model could reproduce the local concentration build-up near the impact point. The processes within the near-wall region leading to this local decrease of dilution are discussed in detail. Additionally, a novel criterion is proposed to predict when the flow reaches a quasi-steady-state. The criterion can be used to manage the computational expenses, especially in simulations with high demanding computing power such as LES.

Article Highlights

- The capability of the LES approach to reproduce the mixing behavior of inclined dense jets was investigated.
- The flow behavior in the near-wall region was analyzed in detail.
- The LES approach was able to predict the flow behavior, especially in the near-wall region, with reasonable accuracy.

✉ Ozeair Abessi
Oabessi@nit.ac.ir

¹ School of Mechanical Engineering, Amirkabir University of Technology, Tehran, Iran

² School of Civil Engineering, Babol Noshirvani University of Technology, Babol, Iran

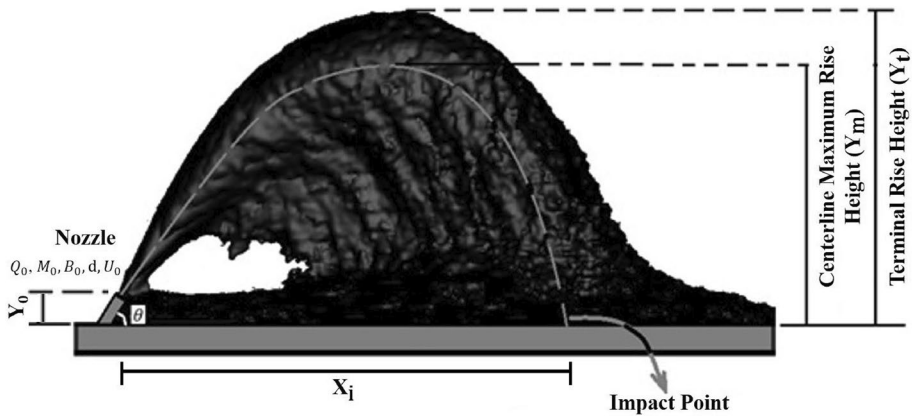


Fig. 1 A view of dense jet flow in stagnant water [1]

Keywords OpenFOAM · Dense jet · Large eddy simulation · Mixing · LIF

1 Introduction

Brine, high-concentration saline water, is a by-product of many industrial processes, but it is mainly considered as effluent from desalination plants. Desalination plants have been risen dramatically in the last decades to supply the increasing water demand for potable and industrial uses [1]. The brine is commonly discharged back into the sea through marine outfalls installed on the seafloor far enough from the shore and ecologically sensitive areas. The discharge with upwardly inclined jets is frequently used for this purpose [1]. The flow in inclined dense jets is fully turbulent, which results in a high mixing rate so that the brine concentration reduces to the safe levels with minimum impacts on marine biota [2, 3].

The dynamics and mixing of the single and multiport dense jets in stationary and flowing environments have been investigated in many studies [4–9]. The dense jet reaches a maximum height and then falls back to the seafloor. After impacting the sea bed, it spreads as a density current. The main flow characteristics and definitions of variables for a single inclined dense jet in a stationary environment are exhibited in Fig. 1. The jet discharges from a round nozzle of diameter d at velocity U_0 , inclined upward at an angle θ to the horizontal plane.

Finding the optimal angle of inclination has long been questioned by engineers and outfall designers. So many experimental and numerical studies have been conducted to respond to that. Cederwall [10] commented that 45° is the optimal angle, and Zeitoun et al. [11] proposed 60° as the angle with the highest dilution compared to the other angles. Based on the latter, Roberts et al. [4] carried out detailed measurements on 60° jets to quantify important properties of inclined dense jets.

The investigation of the effect of nozzle inclination angle is not limited to previously mentioned works. Several other studies, such as Kikkert et al. [6], Jirka [7], Papakonstantis et al. [12, 13], Lai and Lee [8], and Oliver et al. [9] have also conducted experiments to see the effect of nozzle angle. Jirka [7] raised doubts over the proposed angle of 60° through a theoretical study on the dense jets discharging at 0° – 90° angles. Using the integral model

of CORJET, he found that nozzles with angles ranging between 60° and 75° give the highest dilutions for the flatbeds and 30° – 45° for steeply sloping beds. Therefore, Jirka [7] suggested that probably the smaller angle of about 30° – 45° may be optimal. Oliver et al. [9] developed a new set of experimental data and analytical solutions over a wide range of angles from 15° to 75° and proposed 60° as the angle with maximum dilution. Oliver et al. [9] challenged Jirka's [7] results and reported that dilution for 60° is up to two times more than that observed for 30° . Therefore, there was not a universal agreement up to the recent publication of USBR¹ [14] that put an end to this conflict based on comprehensive Three Dimensional Laser-Induced Fluorescence (3D-LIF) experiments that were performed for different nozzle angles. The dependency of flow parameters on the nozzle angle was investigated by Roberts and Abessi [14]. It was found that the impact point dilution is relatively insensitive to nozzle angle over the range of 45° – 65° , while the near-field dilution was found to be more sensitive to nozzle angle with the maximum value for 60° jet. The empirical equations of this study were later verified by the field observation of Antenucci et al. [15], Baum et al. [16, 17].

Antenucci et al. [15] studied Southern Seawater Desalination Plant (SSDP) at Binnigup, south of Perth, Australia, where brine directly discharges back into the ocean via a submerged multiport diffuser. They measured the vertical profiles of conductivity, temperature, dissolved oxygen, pH, and redox potential at five stations and plotted them along with the experimental data. The field data was consistent with the experimental observations of Abessi and Roberts [18]. Baum et al. [16, 17] carried out a comprehensive series of field studies on the Gold Coast Desalination Plant (GCDP) in South East Queensland, Australia. The high-resolution dynamics of brine flow were captured by a three-dimensional array of conductivity and temperature sensors for the measured condition of ambient velocity and wave characteristics. Comparing the results with Abessi and Roberts's [5] data indicated that the geometrical properties were close to the laboratory data while dilution observations were farther from the range reported by Abessi and Roberts [5].

In order to enrich the available experimental data on negatively buoyant jets, Papakonstantis and Tsatsara [19, 20] performed a series of experiments to report the trajectory and mixing properties of those whose inclination angles have rarely been investigated in the literature. Crowe et al. [21] used the Particle Tracking Velocimetry (PTV) method to capture the velocity field for 15° – 75° inclined dense jets to complement previous studies, which have mainly focused on the mean geometric and dilution properties of the fluid flow. Their work presented new insights into buoyant instabilities on the inner half of the dense jets. Ramakanth et al. [22], in a new experimental look at the lower boundary influences on dense jet mixing, investigated flow dilution at common reference points near the boundary. They experimented with different source heights above the boundary and discussed the relationships between the bed proximity parameter and dilution within the impact region. They found that flow diminishes its ability to mix with ambient fluid as it approaches the boundary and this could be up to a 30% decrease compared to the conditions with no boundary influences.

Thanks to recent advancements in computing power, Computational Fluid Dynamics (CFD) has attracted a lot of attention as a valuable tool for studying and designing marine outfalls. Hence, many numerical studies have been reported in the context of dense jets in recent years. Vafeiadou et al. [23] used CFX-5 of ANSYS software with the $k - \omega$ SST

¹ United States Bureau of Reclamation.

(Shear Stress Transport) turbulence model to numerically simulate 60° inclined dense jets in stagnant environments. They found that the model underestimated the terminal rise height and the return point compared to the experimental data of Roberts et al. [4]. The CFX was also used by Oliver et al. [24] to study 60° inclined dense jets using the standard $k - \epsilon$ turbulence model. They tried to enhance the accuracy of the predictions through the adjustment of turbulent Schmidt number in the tracer advection–diffusion equation. Although this calibration improved the predictions of some bulk parameters, the overall effect on the quality of results was small. Therefore, they reported that the numerical model could predict the flow properties no better than integral models of CorJet (Jirka [25]) and VisJet (Lee et al. [26]).

Kheirkhah Gildeh et al. [27] used the Reynolds-Averaged Navier–Stokes (RANS) approach to investigate the mixing properties of 30° and 45° inclined dense jets employing the OpenFOAM finite volume model. They applied RNG $k - \epsilon$, realizable $k - \epsilon$, nonlinear $k - \epsilon$, LRR, and Lunder-Gibson turbulence models, to evaluate the prediction accuracy of each turbulence model. After comparing the results to experimental data, they reported that the LRR and realizable $k - \epsilon$ turbulence models predict the flow properties more accurately. Zhang et al. [28] employed the Large Eddy Simulation (LES) approach with the Smagorinsky and Dynamic Smagorinsky sub-grid models to numerically simulate 45° and 60° inclined dense jets. The results showed that the model was able to accurately predict dense jets' behavior, specifically their bottom interactions along with the spreading layer on the seafloor. However, their simulations underpredicted the impact point dilution but could still reproduce the local concentration build-up at this point that was previously reported by Abessi and Roberts [29]. This local build-up close to the bed forms a rapid variation of dilution at the impingement point. It was found to be an important feature for determining the impact point dilution and probably the cause of the wide discrepancies in reported dilutions in the vicinity of the impact point.

Tahmooreesi and Ahmadyar [30] investigated the effect of turbulent Schmidt number in the tracer advection–diffusion equation on the accuracy of RANS predictions of dense jets. They reported that reducing the turbulent Schmidt number from 1.0 to 0.4 improves the dilution predictions, while this adversely affects the numerical predictions of geometrical properties as well as cross-sectional distributions of concentration. In a recent study, Ramezani et al. [31] investigated the effect of proximity to the bed on the behavior of 30° and 45° inclined dense jets by developing a solver within the CFD package of OpenFOAM. It was observed that proximity to the bed has almost no appreciable effects on the behavior of 45° jets. In comparison, in 30° jets, when the bed proximity parameter falls below 0.14, the normalized values of the horizontal and vertical locations of the centerline peak as well as return point dilution reduce compared to the free condition. Meanwhile, the terminal rise height remains untouched.

There are generally three approaches for turbulence modeling, namely Direct Numerical Simulation (DNS), Large Eddy Simulation (LES), and Reynolds-Averaged Navier–Stokes (RANS). In the RANS approach, all turbulence fluctuations are modeled and represented in terms of the mean flow characteristics. In contrast, the Navier–Stokes equations are directly solved in the DNS approach without any simplifying assumption. The LES approach can be considered as a compromise between DNS and RANS in which the larger eddies of the flow are directly solved, whereas the smaller turbulent motions are modeled [32, 33]. Amongst the mentioned approaches, the RANS is used more widely due to its lower computational costs. While using the DNS approach in many industrial flows, large-scale simulations, or high Reynolds flows is not feasible since, in this approach, all length scales and timescales have to be resolved, which

imposes extremely heavy computational expense. Regarding recent advancements in computing power, the LES approach has drawn ever-increasing attention as a trade-off between accuracy and computational cost.

Reviewing previous works highlights the lack of a comprehensive LES study in the field of dense jets. The earlier studies in this context that used the LES approach are limited to one or two steep angles. Thus, this paper presents the most extensive LES study ever undertaken in the field of dense jets to evaluate the capability of the LES approach to predict their geometrical mixing characteristics, with a particular emphasis on the near-wall region where the most complicated structures of the flow occur. Besides numerical simulations, a series of experiments using the Planar Laser-Induced Fluorescence (PLIF) technique is performed to compare each numerical simulation with its experimental correspondence.

2 Materials and methods

2.1 Governing equations

In the LES approach, different from the RANS models in which only mean-flow data is available as the whole bunch of eddies are modeled, turbulent flow eddies are filtered into large and small eddies based on the local grid sizes. Large eddies are then computed directly by solving the instantaneous Navier–Stokes equations, while smaller eddies are modeled based on the Boussinesq assumption, for instance.

The filtered three-dimensional unsteady Navier–Stokes equations for incompressible flows can be written as follows [34]:

$$\frac{\partial \bar{u}_j}{\partial x_j} = 0 \tag{1}$$

$$\frac{\partial(\rho \bar{u}_i)}{\partial t} + \frac{\partial(\rho \bar{u}_i \bar{u}_j)}{\partial x_j} = -\frac{\partial \bar{p}_{rgh}}{\partial x_i} - gh \frac{\partial \rho}{\partial x_i} + \frac{\partial}{\partial x_j} \left[2\rho(\nu + \nu_{SGS}) \bar{S}_{ij} \right] \tag{2}$$

where \bar{u}_i is the i th component of filtered velocity, x_i is the i th coordinate direction, t is the time, \bar{p}_{rgh} is filtered dynamic pressure, \bar{S}_{ij} is the strain-rate tensor, g is the gravitational acceleration, and h represents the height of the fluid column. The above equations are obtained by employing an implicit filter denoting by the operator “ $\bar{\cdot}$ ” which has an effective width of $\Delta = (V_C)^{1/3}$. ρ and ν are the density and molecular kinematic viscosity of the mixture, respectively, and calculated as:

$$\rho = \alpha \rho_e + (1 - \alpha) \rho_a \tag{3}$$

$$\nu = \alpha \nu_e + (1 - \alpha) \nu_a \tag{4}$$

where α is the volume fraction of effluent, ρ_e is the effluent density, ν_e is the effluent molecular kinematic viscosity, ρ_a is the ambient density and ν_a is the ambient molecular kinematic viscosity. The volume fraction of effluent is calculated through a transport equation, which can be formulated as:

$$\frac{\partial \bar{\alpha}}{\partial t} + \frac{\partial(\bar{u}_j \bar{\alpha})}{\partial x_j} = \frac{\partial}{\partial x_j} \left[\left(D_{ab} + \frac{\nu_{\text{SGS}}}{\text{Sc}_{\text{SGS}}} \right) \frac{\partial \bar{\alpha}}{\partial x_j} \right] \quad (5)$$

where D_{ab} represents the molecular diffusivity and Sc_{SGS} is the turbulent Schmidt number. The ν_{SGS} in Eqs. (2) and (5) is the Sub-Grid Scale (SGS) kinematic viscosity and is employed to reproduce the effect of SGS fluctuations in a diffusive manner. The LES model computes ν_{SGS} using one-equation SGS kinetic energy, k_{SGS} , transport model as [35]:

$$\nu_{\text{sgs}} = C_k \bar{\Delta} k_{\text{SGS}}^{1/2} \quad (6)$$

$$\frac{\partial(k_{\text{SGS}})}{\partial t} + \frac{\partial(\bar{u}_j k_{\text{SGS}})}{\partial x_j} = \nu_{\text{SGS}} (2\bar{S}_{ij}\bar{S}_{ij}) - C_\epsilon k_{\text{SGS}}^{3/2}/\bar{\Delta} + \frac{\partial}{\partial x_j} \left(\nu_{\text{SGS}} \frac{\partial k_{\text{SGS}}}{\partial x_j} \right) \quad (7)$$

Here the dynamic LES model proposed by Kim and Menon [36] takes advantage of a test filter with a double-length, $\bar{\Delta} = 2\Delta$ to compute C_k and C_ϵ .

2.2 Numerical methods

The simulations are performed using the *twoLiquidMixingFoam* solver of the finite volume open-source package of OpenFOAM. This is a solver for the mixture flow of two incompressible fluids. The solver uses the PIMPLE (Semi-Implicit Method for Pressure-Linked Equations) algorithm for pressure–velocity decoupling of the Navier-Stokes equations. As a combination of the SIMPLE and PISO (Pressure-Implicit with Splitting of Operators) algorithms, the PIMPLE algorithm allows using larger Courant numbers and larger time intervals for the simulation of unsteady flows. For further information about the PIMPLE algorithm, please refer to Holzmann [37]. Here, the second-order accurate central differencing scheme is used for the discretization of the diffusion terms. Using central differencing for convection terms may lead to unphysical oscillations, and it is usually avoided [38]. Using upwind-dominated schemes by creating numerical dissipations of the order of SGS viscosity dissipation may dampen flow turbulences and decrease LES accuracy [39]. Therefore, convection terms are discretized using the Gauss filtered Linear, a second-order central differencing scheme in OpenFOAM with added small amount of local upwinding [40]. The Van Leer scheme [38] is used for the discretization of the transfer equation of effluent volume fraction. The Second-Order Upwind Euler (SOUE) scheme is also used for the discretization of temporal terms [41]. Temporal steps were variable with a maximum Courant number of 0.5 throughout the simulations. For time averaging, each case is run to reach a developed quasi-steady condition and then run for more than 45 s to reach a time-averaged image of the flow features.

A computational domain with dimensions of 2.4 m long, 0.92 m wide, and 0.61 m deep was chosen based on the known behavior of the flow and experimental setup (Fig. 2). The nozzle was located 0.5 m from the tank side; therefore, it had 1.9 m of space in front of it to develop. As shown in Fig. 2, the simulation is performed with a grid of 5,500,000 cells with finer grids near the nozzle for better accuracy. Five levels of refinement have been considered with the cell size of 0.014 m in level 0, 0.007 m in level 1, 0.0035 m in level 2, 0.00175 m in level 3, 0.000875 m in level 4, and a minimum size of 0.0004375 m in level 5.

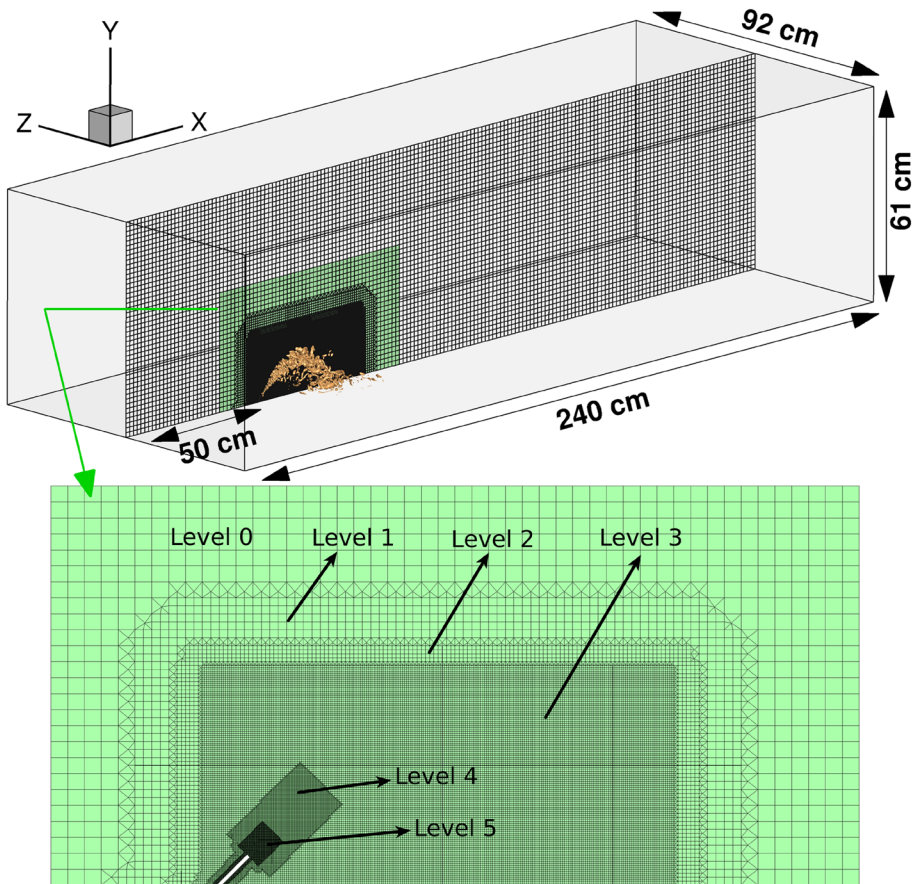


Fig. 2 The geometry and computational grid

The resolution of the computational grid strongly affects the result of LES. The resolution quality of the LES simulation can be determined with some criteria named the “LES indices of Resolution Quality (LES_IQ_k).” One of them is defined as the ratio of the resolved part of the turbulent kinetic energy (TKE) to the total TKE and can be written as:

$$M = \frac{k_{Res}}{k_{Res} + k_{SGS}} \tag{8}$$

where k_{Res} and k_{SGS} are the resolved and sub-grid scale parts of turbulence kinetic energy, respectively. Celik et al. [42] suggested $M = 0.77–0.85$ to ensure that the grid resolution is fine enough. Pope [43] also considers a grid resolution appropriate if the $M \geq 0.8$. In Fig. 3, M is shown in the cross-section inside the domain. As shown in this figure, the M is higher than 0.8 in the whole domain except for a small area in front of the nozzle indicated by the circle.

The fully developed velocity profile along with zero pressure gradient was considered for the nozzle inlet. The slip condition was imposed for the upper part of the jet,

Fig. 3 The ratio of the resolved part of the TKE to the total TKE

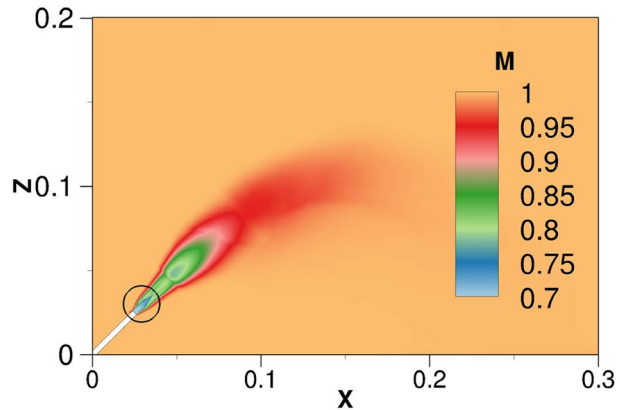


Table 1 The flow characteristics in LES and LIF simulations

Flow characteristic	LES	LIF
<i>Physical characteristics</i>		
Discharge angle	15, 30, 45, 60, 75	15, 30, 45, 60, 75
Nozzle diameter	3.25 mm	3.25 mm
The height of nozzle tip	2.5 cm	2.5 cm
Jet velocity	0.6338 m/s	0.6338 m/s
Turbulent Schmidt number (Sc_{SGS})	0.7	–
Molecular diffusivity (D_{ab})	$1.89 \times 10^{-9} m^2/s$	–
Dynamic viscosity (μ_a)	0.001 Pa*s	0.001 Pa*s
Kinematic viscosity (ν)	$\nu_e = \nu_a = 1.004 \times 10^{-6} m^2/s$	$\nu_e = \nu_a = 1.002 \times 10^{-6} m^2/s$
Effluent density (ρ_e)	$1019.375 kg/m^3$	$1020.99 kg/m^3$
Ambient density (ρ_a)	$998.402 kg/m^3$	$998.25 kg/m^3$
<i>Dimensionless numbers</i>		
Modified acceleration (g')	20.6	22.36
Reynolds number (Re)	2051.64	2100
Densimetric Froude number (Fr)	24.5	23.52
Momentum-buoyancy length scale, cm, (L_M)	7.48	7.18

while the no-slip condition was considered for wall boundaries, i.e., the lateral boundaries and floor. In addition, for wall boundaries, the *zeroGradient* boundary condition was chosen for pressure. For open boundaries, namely upstream and downstream, the *totalPressure* and *pressureInletOutletVelocity* boundary conditions were considered for velocity and pressure, respectively. Such compositions are proposed for open boundaries with inflow by the OpenFOAM user guide [44]. The characteristics used for the simulations are summarized in Table 1. The characteristics used for the simulations are summarized in Table 1.

2.3 Experimental methodology

To calibrate and verify the LES results, the PLIF technique has been used to measure the spatial evolution and mixing processes of the inclined dense jets at each angle. This is a laser-based optical measurement technique for determining concentration or temperature in the flow field. It is individually developed and upgraded by different scholars around the world. The apparatus and codes used in this study are similar to those developed by Tian and Roberts [45]; however, they have been upgraded in the present setup to be able to capture and process the concentration fluctuations. It can capture a three-dimensional picture of the flow; however, the planar measurements on the central plane were only used in this study. The method of experimental analysis has been described in several publications by Tian and Roberts [45], Abessi and Roberts [18], and Abessi et al. [46].

In our experimental setup, a glass-made tank with 2.8 m length, 1.5 m width, and 1 m depth equipped with LIF apparatus was used to perform the experiments. This system was established and outfitted in the Environmental Fluid Mechanics laboratory of the Babol Noshirvani University of Technology and used in this study to illuminate the mixing and spatial behavior of the inclined dense discharge at various angles. The system consisted of two swift scanning mirrors to provide a flat laser sheet across the centerline of the flow. The laser sheet was formed by the oscillation of a 200 milliwatts green Diode-pump solid-state laser (DPSSL) beam with 0.5 mm width. With an infinitesimal quantity of a fluorescent dye (Rhodamine 6G, Sigma-Aldrich, St. Louis, Missouri), the discharged effluent would be fluoresced under the impression of the laser. The emitted light is captured by a CCD camera (Mars 640-300G 1/4 “@4.8um) in the grayscale form at the rate of 100 frames per second. The procedures were controlled by a computer server equipped with an I/O board and controlling software. The images were continuously downloaded to the hard disk of the server for later processes. The captured images were then modified and calibrated for laser attenuation and sensor response for each pixel using clear and dyed water of known concentration. The same method that was followed to extract tracer concentrations from the images is discussed in Tian and Roberts [45]. The process was first described by Daviero et al. [47] and then used in many other studies of the same team, such as Gungor and Roberts [48], Abessi and Roberts [18], and Fedele et al. [49]. The accuracy of the dilution measurements was calculated at about 10% [46]. The stream of images for the unsteady flow was captured long enough to make sure that the jets reached quasi-steady conditions. This time was identified empirically in the lab by observing the time evolution of the flow. By reaching the quasi-steady flow, the images were recorded for at least 45 s and then time-averaged to reach the steady planar view of the flow at the centerline. The same conditions are used later in the LES study for the numerical simulation and time averaging of the flow.

The effects of the tank walls can always be an issue. The experiments were conducted with a raised false floor. The false floor does not extend the full tank length and width, so the density current runs over the edge and does not begin to fill the tank or reflect back within the duration of the experiments. Therefore, the spreading layer does not rapidly impact the side-walls, and it makes us sure that the flow has space to propagate on the floor.

3 Dimensional analysis

The dimensional analysis of free dense jets is a well-known case and has been described in previous studies (e.g., Fischer et al. [50] and Roberts et al. [4]). According to the mentioned studies, the dependent variables of the flow φ , can be characterized by the jet kinematic fluxes of volume $Q_0 = \frac{\pi}{4}d^2U_0$, momentum $M_0 = U_0Q_0$, buoyancy $B_0 = g'_0Q_0$ and the discharge angle θ :

$$\varphi = f(Q_0, M_0, B_0, \theta) \quad (9)$$

where $g'_0 = g(\rho_0 - \rho_a)/\rho_a$ is the modified acceleration due to gravity. These fluxes are used to develop the jet-to-plume transition length scale $L_M = M_0^{3/4}/B_0^{1/2} = \left(\frac{\pi}{4}\right)^{0.25} Fr_d d$ where $Fr_d = U_0/\sqrt{g'_0 d}$ is the jet densimetric Froude number. Roberts and Toms [51] expressed that the effect of volume flux, Q_0 lose its importance for high densimetric Froude numbers ($Fr_d > 20$). Therefore, all the dependent variables φ will only be a function of M_0 , B_0 , and θ . By dimensional analysis, it can be shown that a characteristic length χ and dilution S can be nondimensionalized with L_M (or $Fr_d d$), and densimetric Froude number Fr_d as follows:

$$\frac{\chi}{L_M} = f(\theta), \quad \frac{S}{Fr_d} = f(\theta) \quad (10)$$

where dilution is defined as $S = (C_0 - C_a)/(C - C_a)$ where C_0 , C_a , and C are jet discharge concentration, ambient concentration, and local time-averaged concentration, respectively.

It is worth mentioning that the ambient depth H (more precisely, the distance of the nozzle tip to the water surface) and the distance of the nozzle tip to the lower boundary y_0 can potentially affect the flow behavior [31, 52–55]. In the present study, however, in order to avoid possible influences of surface contact and the Coanda effect on the flow behavior, enough distance from the surface and seafloor was considered in both experimental and numerical simulations based on the criteria reported by Abessi and Roberts [52], Shao and Law [53] and Ramezani et al. [31, 55].

4 Results and discussion

4.1 General observations

By solving the instantaneous Navier–Stokes equations for larger eddies in LES, concentration contours were obtained and presented in Fig. 4 for different nozzle angles. The time-averaged image of concentration for each angle is also plotted in the same figure. Time-averaged and instantaneous tracer field images from LIF experiments are presented in Fig. 5. A few seconds after the beginning, the flow reaches its maximum rise height due to initial discharge momentum. Negative buoyancy drives the jet back to the seabed, where it spreads as a density current. This process leads to a longer trajectory and higher dilution for inclined nozzles compared to vertical jets and helps to clear density current from the discharge site. The location of bed impingement is the first and probably the most important point in the process of brine discharge, as this is the first point of brine contact with

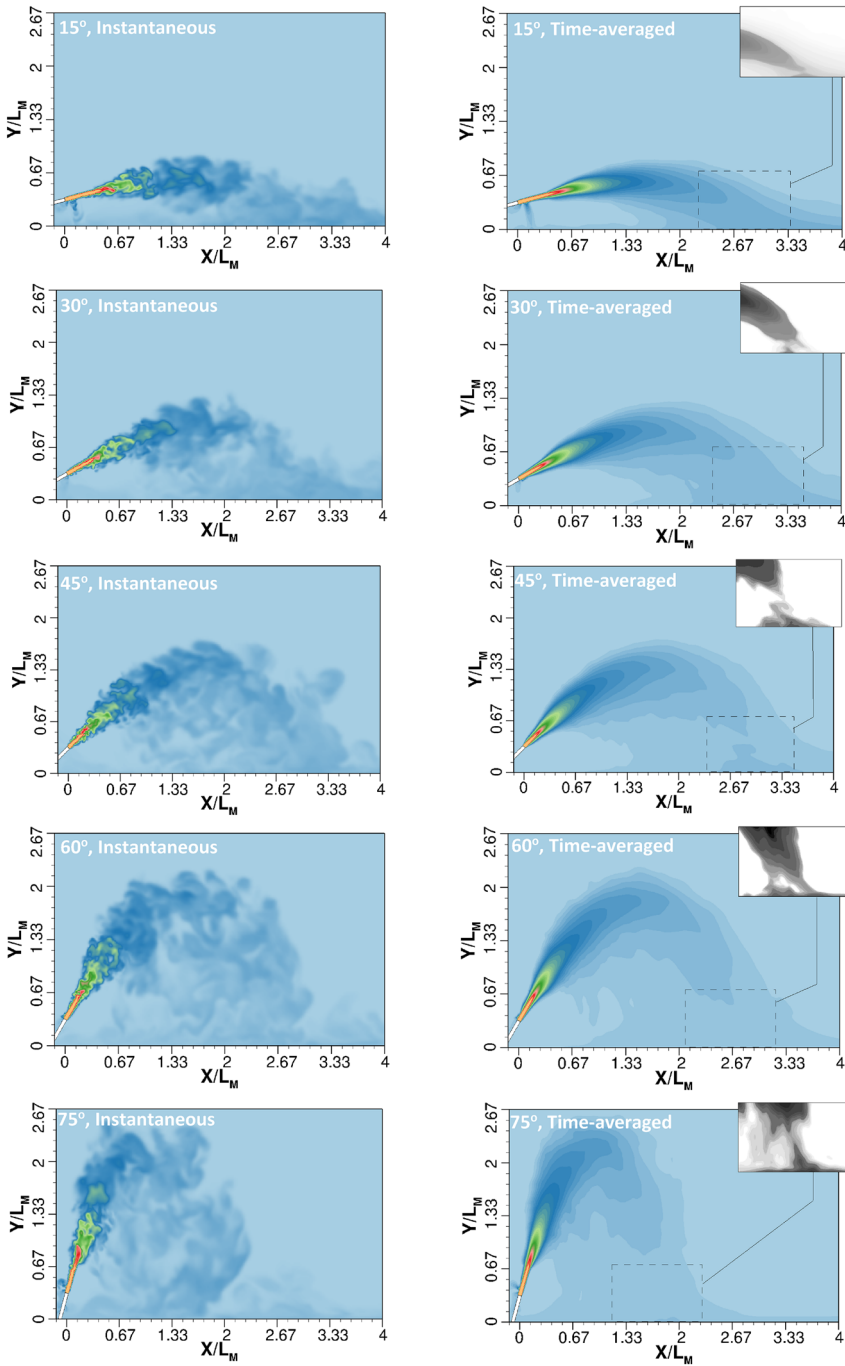


Fig. 4 LES results for tracer concentration ($\mu g/l$) along the centerline for various nozzle angles; instantaneous and time-averaged figures as specified in left and right-hand panels

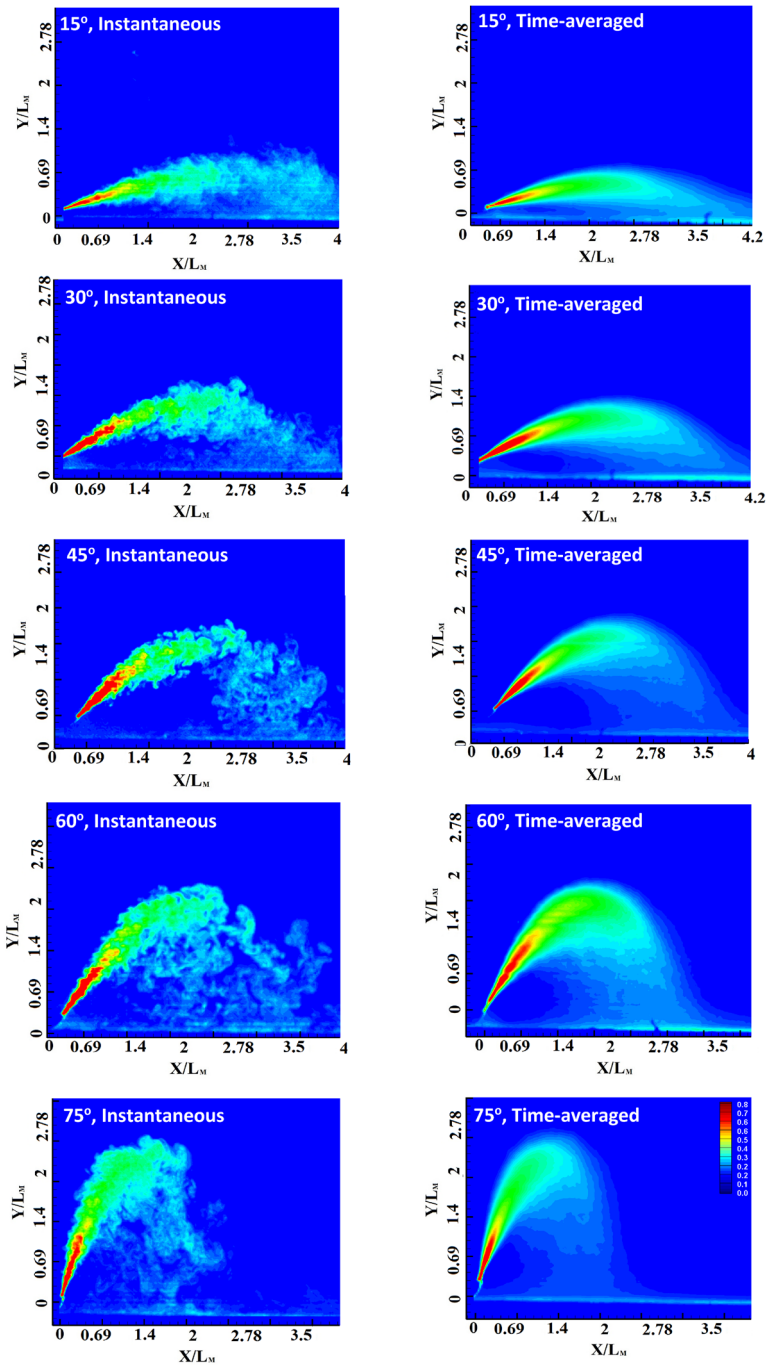


Fig. 5 Experimental observation for tracer concentration along the centerline for the various nozzle angle; instantaneous and time-averaged figures as specified

benthic organisms. This location also corresponds to the lowest seabed dilution as the flow dilutes more by the act of vortices from this point. The vortices on the floor entrain more ambient water into the jet and eventually collapse under their self-induced density stratification downstream of this area, as first explained by Roberts et al. [4] and elaborated by Abessi and Roberts [29]. This region marks the end of the initial mixing zone or the location of the near field, which is an important location where water quality standards must generally be met. As shown, jet concentration decays along the path due to the entrainment and mixing that begin right after the nozzle tip. The mixing is attributed to the instabilities of shear-induced entrainment on the jet circumferences, which get bigger at the jet's lower half by the acts of peeling detrainment. This buoyancy-induced instability (detrainment) leads to a distinctive asymmetry in the cross-sectional mean profile from the inner to the outer side. This was reported as the main reason for special flow behavior in inclined dense discharges and was well-described in previous works [9].

The LES model could also show the local concentration build-up at the location of the impact point. It is illustrated in the time-averaged of concentration field in Fig. 4. This phenomenon is probably the reason for the unexpected concentration variations near the bottom boundary in reported works. This behavior first has been observed in the experimental simulations (Fig. 5) and reported by Abessi and Roberts [29]. This is explored further below in Sect. 4.3.

In the laboratory, the detailed structures of the flow can easily be identified as no modeling or averaging is applied for the smaller structures. In the current experiments, the camera captured the time scale down to 0.01 s (100 Hz) and the length scale down to 0.00025 m, comparably higher than the dimension of the minimum sub-grid scale in the LES model (Level 5 in Fig. 2). With better technology of high-speed camera with 4 K resolution, the smaller time and length scales down to the order of 0.002 s, and 0.00001 m is now accessible. So, it can be used to see the scales of inertial subrange down to about the Kolmogorov scale.

In Fig. 4, the eddy structures of LES results are visualized by plotting the instantaneous contours for concentration in a diverging color map at the central plane. The eddy structure at the same plane was exhibited for the PLIF results in Fig. 5. Instantaneous contours were compared with the time-averaged image to make them comparable with each other and previous works. By comparing the LES results to the snapshot of the flow in the laboratory, it can be inferred that LES is modeling small structures as only bigger eddies are detectable. These eddies were estimated to have up to 80% of the flow energy and are responsible for most flow mixing and dilution.

In both experimental and CFD simulations, it is important to find out the time evolution of flow to reach the moment needed to start time-averaging. In the laboratory, it begins when the lab expert visually sees the flow has developed up to the desired point, and it is different for each angle and differs from the impact point to the location of the near-field as the second happens later. There are limitations for performing long experiments in the laboratory regarding the size of the tank, which gets full of dye tracer, and also in numerical simulations regarding required computational costs.

In Fig. 6, the time evolution of flow for LES results has been demonstrated. For inclined dense jet at 15°, the flow reaches to impact point at 7.5 s, and this happens for 30°, 45°, 60°, and 75° jets at 10, 12.5, 15, and 17.5 s in order. Therefore, modeling should last at least 20–40 s depending on nozzle orientation, and then time averaging needs to be started. However, if the near-field location is intended, a much longer simulation is needed for the flow to reach this point, and then time-averaging should be started. For LES, with such an enormous calculation cost, computer simulation is highly demanding and takes up

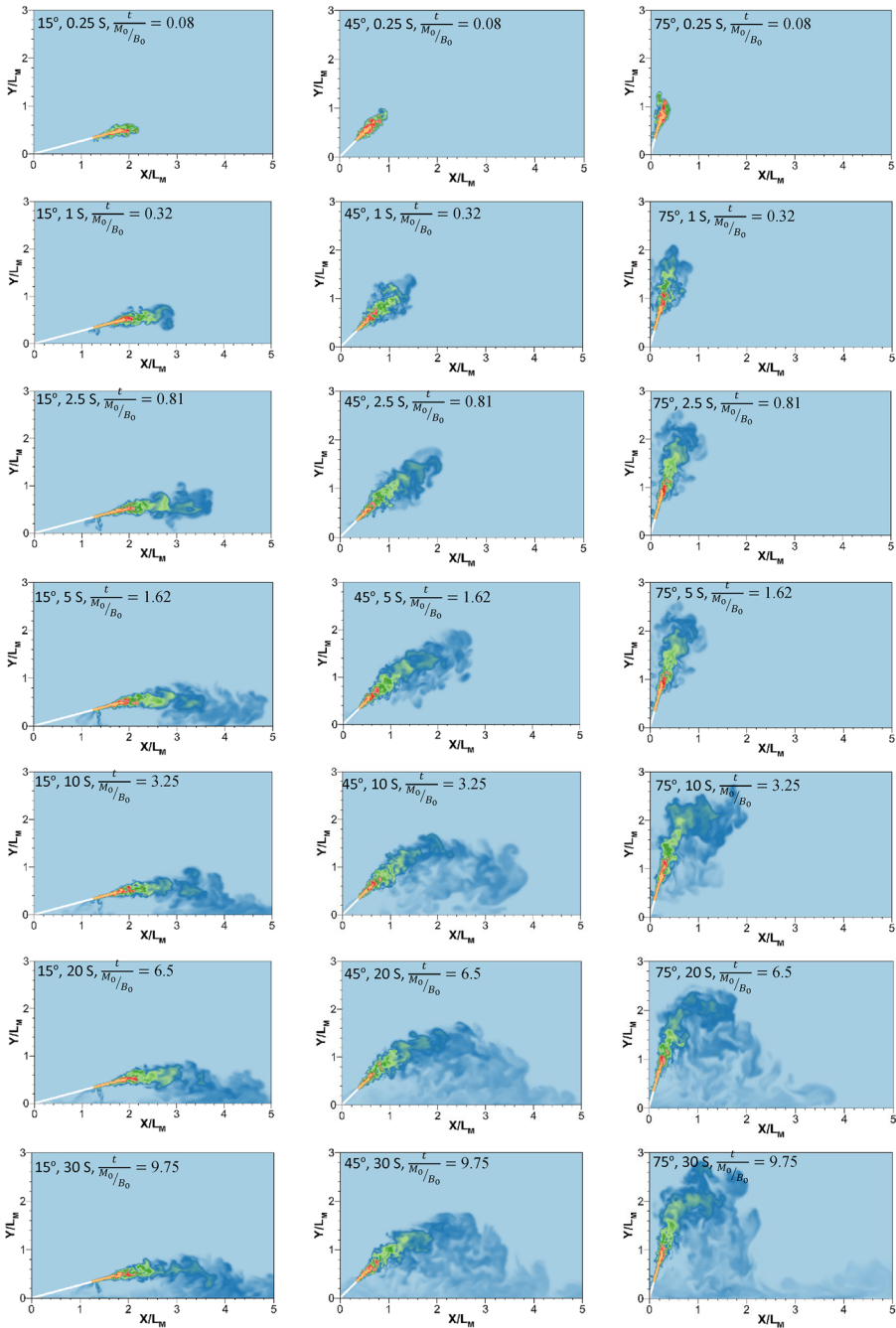


Fig. 6 Flow development in time for inclined dense discharge at 15°, 45° and 75° for $T^* = \frac{t}{M_0/B_0} = 0.08, 0.32, 0.81, 1.62, 3.25, 6.5$ and 9.75 from the beginning (top to bottom)

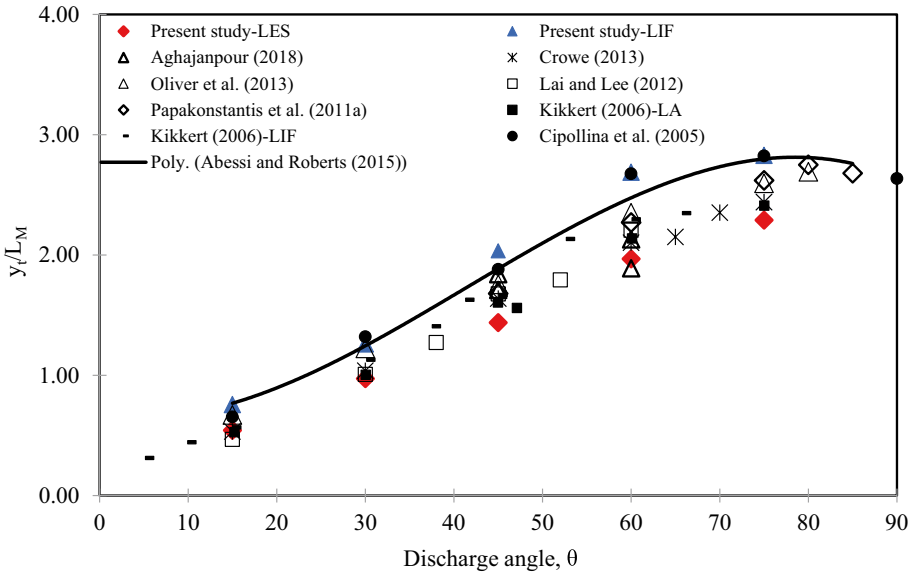


Fig. 7 Terminal rise height for various nozzle angles compare to experiments and previous studies

to several weeks with our best available system. Thus, an initial guess of when the flow reaches the quasi-steady-state is essential for managing the computational expenses and choosing the suitable numerical approach based on desired accuracy and available computing power. Besides jet orientation, the time that flow reaches a quasi-steady-state depends on both initial momentum and buoyancy fluxes. Hence, the times have been non-dimensionalized with M_0/B_0 for each angle in Fig. 6. This can help to guess the time evolution of inclined dense jets based on their initial characteristics.

4.2 Jet trajectory and geometrical features

The major flow parameters of design interest are jet terminal rise height, centerline maximum rise height, and the location of the impact point (Fig. 1). Predicting these parameters is essential in the environmental impact assessment process of brine discharge. Finding the jet rise height is crucial to see if the flow can reach the water surface and cause visual disturbances. The location of the impact point is also the first location where the regulation of maximum concentration should be met, while the end of the near-field is the point of concern in some other standards. In the figures below, these parameters were extracted from the 2D planar concentration fields of LES and LIF and compared to each other. Some other experimental data from the previous studies were also included for comparison.

In Fig. 7, the LES results for the jet terminal rise height were normalized and plotted for various nozzle angles together with our new set of LIF experiments and previous data [8, 9, 12, 29, 56–59]. Following the definition of Roberts et al. [4], this point is defined as the location of 10% of the transverse maximum concentration at the jet's maximum height. The predictions of the LES model are close to those from Lai and Lee [8], Oliver et al. [60], and Kikkert [58] and lower than the results of the present LIF experiments and Abessi

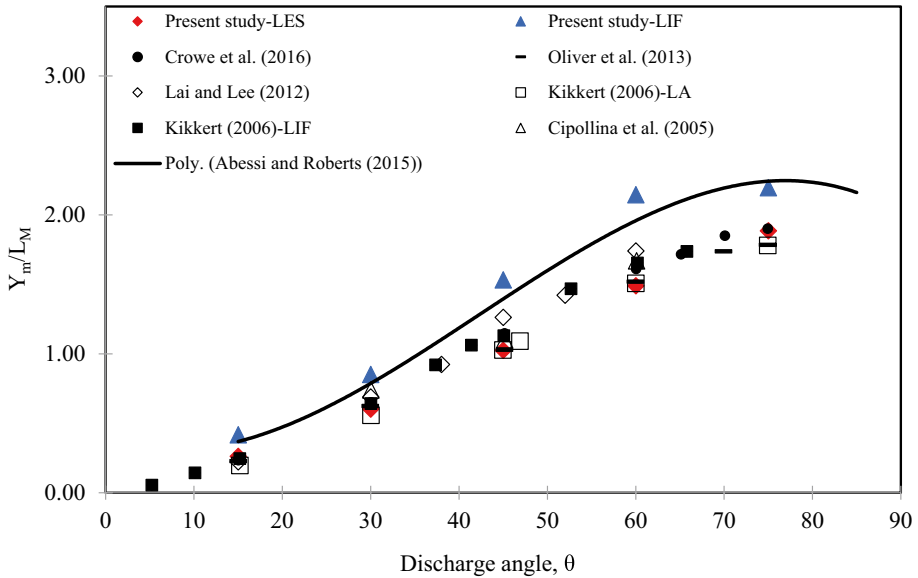


Fig. 8 Centerline maximum rise height for various nozzle angles compare to experiments and previous studies

and Roberts [29]. It is also seen that the discrepancy between the numerical predictions and experimental data gets bigger when the angle of inclination increases.

Jet terminal rise height is also an important feature to define the possibility of deep, surface contact, and shallow regimes [52]. Once the upper side of the jet touches the water surface (surface contact regime), dilution begins to reduce as entrainment from the upside of the jet will be stopped. The mixing is reduced even more when the jet centerline reaches the water surface (shallow water condition).

Jet maximum rise height at the centerline for various nozzle angles is plotted in Fig. 8 and compared to LIF experiments and previous data. As shown, the LES predictions for different angles were lower than the experimental observations. However, LES predictions were close to Lai and Lee [8], Crowe et al. [21], Oliver et al. [60], and Kikkert [58]. If the jet impacts the surface, the water available for dilution may decrease, and the flow dynamics will change [52, 53]. It will change the locations of the impact point and near-field and will decrease dilutions at these points [52]. On submerged dense jets, the recommendations for the shallow condition are based on the rise height to the jet's upper boundary. Abessi and Roberts [52] proposed $dFr_d/H = 0.8, 0.48, \text{ and } 0.42$ where H is the ambient depth, as the criteria from which the surface contact happens and $dFr_d/H = 1.15, 0.7, \text{ and } 0.64$ as the criteria of reaching to shallow water regime for $30^\circ, 45^\circ, \text{ and } 60^\circ$ jets, in order. Following the fact that L_M is equal to $\left(\frac{\pi}{4}\right)^{1/4} dFr_d$ or $L_M = 0.94dFr_d$, anticipating the height of jet centerline maximum and terminal rise height can be used to predict the possibility of surface contact and shallow water regime. It is a crucial parameter in the sitting of brine out-fall in the low sloped seabed, as reaching to proper depth demand costs tremendously.

The impact point X_i , is the intersection of flow with the lower boundary and slightly differs from the return point. The return point is defined as the location where the flow returns to the nozzle elevation. The difference between these two points would be remarkable if the

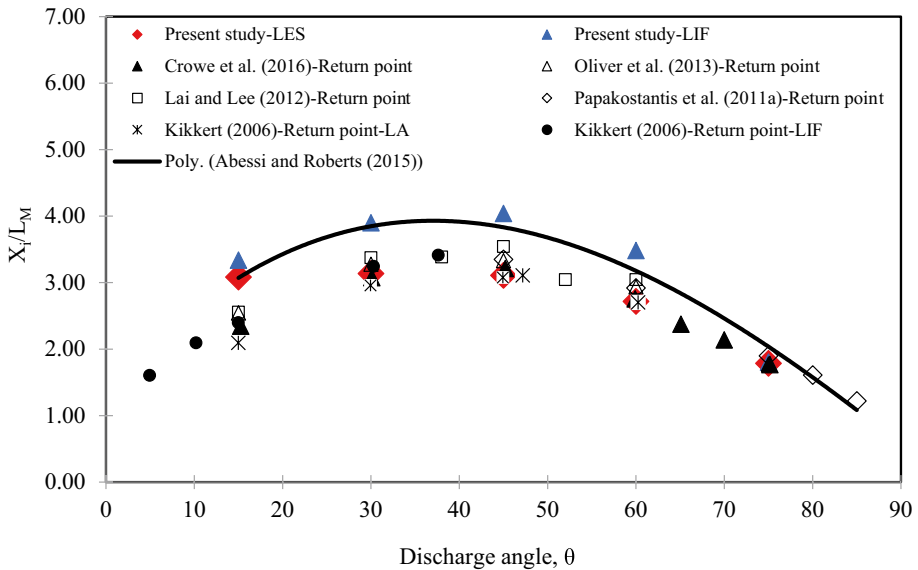


Fig. 9 The horizontal distance of impact point for various nozzle angles

nozzle height is distinctive or the seabed is highly sloped. Therefore, high discrepancies in dilution measurements around the return and boundary impact points were reported in the previous studies [4, 8, 9, 54].

Many of these experiments were conducted with an elevated nozzle tip with flow properties only investigated up to the return point, so they did not account for any boundary influences. This is the region of interest for brine discharges in national standards of many countries as the water quality standards must typically be met there. Therefore, the revelation of the mixing process very close to the bed is essential here. Although the impact point has more practical importance than the return point as the latter is up in the body of ambient water, and no standard goes to this point, many studies reported the location and dilution of the return point instead of the impact point, mainly for two reasons. First, the dilution calculation at this point is pretty straightforward compared to the impact point. And the other, this is more convenient for validation of models as this point is independent of the nozzle height and bed slope. In the present study, however, we put our emphasis on the impact point as the most complicated structures of flow occur at this point, and previous works have rarely investigated it in acceptable detail.

In Fig. 9, the horizontal location of the impact point was plotted against the discharge angle as the non-dimensional parameter of X_i/L_M . The LES model was able to predict the general trend between the location of the impact point and the nozzle angle. However, the model predictions are also shown to sit below the experimental data from the current study and from Abessi and Roberts [29]. It is worth noting that LES predictions are close to other experimental data, regarding the fact that those data are for the return point, which is clearly at a closer distance to the source. Interestingly, the predictions also get closer to the experimental data as the angle increase. Both LES and experimental results show that the maximum horizontal distance to the impact point occurs for 30°–45° jets. Considering that the maximum dilution values have been reported for 45°–60° jets, it can be concluded that jet impingement at a longer distance to the source does not necessarily give more dilution.

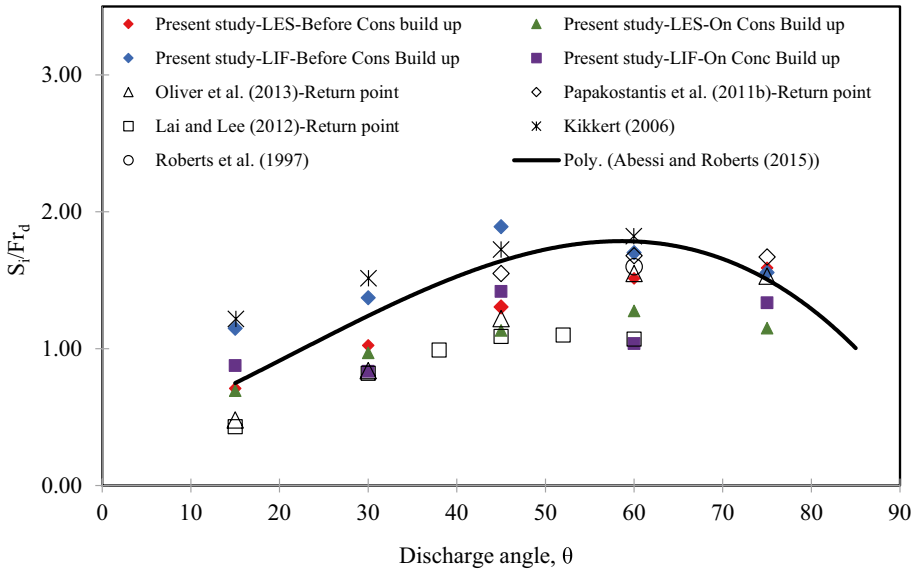


Fig. 10 Dilution at impact point for various nozzle angles

This is because of the different mechanisms of entrainment along the jet and plume regions in rising and falling phases. It is worth mentioning that Zeitoun et al. [11] attributed the dilution to the total length of the trajectory and justified the higher dilution of 60° jets compared to 30°, 45°, and 90° jets by this argument.

4.3 Jet mixing and dilution

Figure 10 shows the LES and LIF results for dilution at the impact point when normalized by Fr_d compared to the previous data. The dilution is defined as the initial concentration of the tracer at the source over the local concentration, C_0/C . As mentioned, dilution at the impact point is the criterion that needs to be met in many discharge standards. The benthic organism has a limited ability to tolerate salinity above the background, and the impact point is the first point of brine contact with the seabed. The data in Fig. 10 shows that the LES results are lower than their LIF counterparts but close to data reported by Lai and Lee [8] and Oliver et al. [60]. Wide discrepancies were reported in the literature for dilutions near the boundary, as the influence of the boundary on dilution measurements is unknown. Abessi and Roberts [29] observed that time-average dilution first increased and then decreased in a thin layer near the wall along the centerline. Due to the law of physics, the concentration value should always decrease while the time-averaged value seems to be increased there. It was found to be due to the increases in turbulent intermittency and accumulation of the saline elements on the lower boundary. It is worth noting that in the impinging region, the brine flow is re-directed from an axial into a radial direction. So the impinging region is composed of the classical stagnation zone where the axial velocity decreases down to zero. The stagnation region is an interesting area for heat dissipation and is well-documented in previous studies [61]. The fluid motion near the stagnation region exists on a solid body when the fluid moves towards it. The stagnation region encounters

the highest rate of mass deposition, and it seems to make the concentration caught in this region.

Such a phenomenon was also observed in the lab for a simple plume when discharging vertically downward with high salinity and low Reynolds number [14]. Extremely like discharging honey in a tank of water. By reaching the bottom boundary, honey loses its momentum and rests on the floor. Therefore, an accumulation of heavy viscous fluid on the floor will be observed. Such a honey effect seems to happen for brine discharge along the plume region, where lower momentum is available to quickly sweep up the heavy fluid away from the impact point. Thus, the brine fluid corresponding to the highest concentrations lays adjacent to the bed and only moves slowly away. Abessi and Roberts [29] elaborated that such a boundary increase in time-averaged concentration is due to the increases in intermittency factor and sorting of the heavier and higher tracer concentration of fluid elements near the bed. It is probably the main reason for the sudden increase in concentration and discrepancies in reported dilutions at the impact point. Zhang et al. [28] mentioned that they could simulate the local concentration build-up at the impact point in their LES model. As mentioned above, such a sudden increase in concentration was observed in our LES and LIF results, too (Figs. 4 and 5). The tracer concentration right before this jump and at the point of concentration build-up was used to measure dilution for the LES and LIF results in Fig. 10. It is clear that if the dilution at the concentration build-up is considered, we will reach a lower dilution for both models, and it was more distinctive in our experimental observations. Interestingly, even before the concentration buildup, the LES model predicts a reduction in mixing at the location of return point. It is probably the source of the high discrepancy reported for brine dilution at both return and impact point, and scholars should pay more attention to the validity of dilution measurements at this point. It is worth noting that no previous numerical work that used the RANS approach could reproduce the concentration build-up at the impact point, even those that used low-Reynolds turbulence models such as $k-\omega$ SST, which allow integration up to the wall without employing wall functions [28, 31, 62, 63]. This clearly shows the higher resolution and accuracy of the LES approach than widespread RANS models in near-wall regions.

As mentioned earlier, Ramakanth et al. [22] have recently argued that dilution after the return point will be significantly affected by the lower boundary. By plotting center-line concentration over time at various points between the return point and the bed, they have tried to quantify the relationship between the bed proximity parameter and dilution at the impact region. Authors believe that the complex process of mixing and entrainment near the boundary definitely needs further investigation, both experimentally and numerically. We suggest a DNS or a high-resolution experimental study focusing on this region for exploring the physics of entrainment and the changes in turbulence properties for the region close to the bed.

The geometrical and dilution results of the present study, along with various past experimental, analytical, and numerical works, were quantified in Table 2 for better comparison. It is seen in the table that the present LES model predicts the geometrical and dilution properties of dense jets with reasonable accuracy. It can be inferred from the table that the accuracy of the LES model is higher than analytical solutions such as the well-known integral model of CorJet and also lower-resolution RANS models, especially in dilution predictions. However, similar to most integral and numerical models, the LES model underestimates the flow features in comparison to experimental data. This underestimation is seen more noticeably in dilution results as it predicts the dilution properties up to 25% lower than the average of experiments. Therefore, more efforts are still needed in the area of numerical modeling of negatively buoyant jets to improve the predictions.

Table 2 Summary of numerical results with previous experimental, analytical, and numerical data

Jet angle		15°	30°	45°	60°	75°
Study	Description					
<i>Terminal rise height (y_t/dFr_d)</i>						
Present study	LES	0.58	1.03	1.53	2.09	2.43
Present study	LIF	0.80	1.34	2.16	2.86	3.00
Crowe et al. [21]	PTV	0.57	1.09	1.73	2.23	2.59
Abessi and Roberts [29]	3D-LIF	0.82	1.31	2.03	2.54	2.93
Oliver et al. [60]	LIF	0.63	1.15	1.65	2.21	2.53
Lai and Lee [8]	LIF/PIV	0.44	0.95	1.58	2.08	–
Papakonstantis et al. [12]	Visual/Probe	–	–	1.59	2.15	2.48
Kikkert [58]	LA	0.57	1.06	1.71	2.28	2.57
Kikkert [58]	LIF	0.60	1.20	1.78	2.45	–
Kikkert et al. [58]	Analytical	0.54	1.07	1.66	2.27	2.84
CorJet (data from [7])	Integral model	0.52	0.95	1.48	1.93	2.19
Ramezani et al. [31]	RANS	–	0.95	1.47	–	–
Zhang et al. [28]	RANS	–	–	1.04	–	–
<i>Vertical location of centerline peak (y_m/dFr_d)</i>						
Present study	LES	0.28	0.64	1.09	1.58	2.00
Present study	LIF	0.44	0.90	1.63	2.28	2.33
Crowe et al. [21]	PTV	0.25	0.69	1.22	1.71	2.02
Oliver et al. [60]	LIF	0.24	0.66	1.09	1.61	1.89
Lai and Lee [8]	LIF/PIV	0.21	0.65	1.19	1.64	–
Papakonstantis et al. [13]	Visual/Probe	–	–	1.17	1.68	1.93
Kikkert [58]	LA	0.22	0.60	1.09	1.60	1.90
Kikkert [58]	LIF	0.26	0.69	1.21	1.76	–
Kikkert et al. [58]	Analytical	0.23	0.63	1.14	1.70	2.23
CorJet (data from [7])	Integral model	0.20	0.56	0.99	1.38	1.65
Oliver et al. [67]	Integral model	0.25	0.63	1.14	1.66	2.15
Crowe et al. [68]	Integral model	0.23	0.63	1.12	1.58	1.94
Ramezani et al. [31]	RANS	–	0.59	1.03	–	–
Zhang et al. [28]	RANS	–	–	0.72	–	–
<i>Horizontal distance of impact point (x_i/dFr_d)</i>						
Present study	LES	3.28	3.33	3.30	2.89	1.90
Present study	LIF	3.55	4.14	4.29	3.70	1.92
Crowe et al. [21]	PTV	2.51 (r)	3.56 (r)	3.43 (r)	2.93 (r)	1.87 (r)
Oliver et al. [60]	LIF	2.39 (r)	3.08 (r)	3.13 (r)	2.76 (r)	1.67 (r)
Lai and Lee [8]	LIF/PIV	2.41 (r)	3.18 (r)	3.34 (r)	2.84 (r)	–
Papakonstantis et al. [12]	Visual/Probe	–	–	3.16 (r)	2.75 (r)	2.51 (r)
Abessi and Roberts [29]	3D-LIF	3.23	4.06	4.08	3.38	1.95
Kikkert [58]	LA	2.30 (r)	3.17 (r)	3.31 (r)	2.78 (r)	–
Kikkert [58]	LIF	2.59 (r)	–	–	–	–
Kikkert et al. [58]	Analytical	2.41 (r)	2.96 (r)	3.05 (r)	2.72 (r)	1.88 (r)
CorJet (data from [7])	Integral model	1.90 (r)	2.53 (r)	2.62 (r)	2.23 (r)	1.29 (r)
Oliver et al. [67]	Integral model	2.24 (r)	2.95 (r)	3.12 (r)	2.89 (r)	2.05 (r)
Crowe et al. [68]	Integral model	2.30 (r)	2.95 (r)	3.08 (r)	2.67 (r)	1.76 (r)

Table 2 (continued)

Jet angle		15°	30°	45°	60°	75°
Study	Description					
Ramezani et al. [31]	RANS	–	2.97 (r)	3.02 (r)	–	–
Zhang et al. [28]	RANS	–	–	2.97	–	–
<i>Impact point dilution (S/Fr_d)</i>						
Present study*	LES	0.71/0.69	1.02/0.97	1.30/1.13	1.51/1.28	1.59/1.15
Present study**	LIF	1.15/0.88	1.37/0.83	1.89/1.42	1.70/1.04	1.56/1.34
Lai and Lee [8]	LIF/PIV	0.43 (r)	0.82 (r)	1.09 (r)	1.07 (r)	–
Papakonstantis et al. [13]	Visual/Probe	–	–	1.55 (r)	1.68 (r)	1.67 (r)
Abessi and Roberts [29]	3D-LIF	0.76	1.16	1.65	1.75	1.50
Oliver et al. [60]	LIF	0.48 (r)	0.84 (r)	1.22 (r)	1.55 (r)	1.53 (r)
Kikkert et al. [58]	Analytical	–	0.68 (r)	0.96 (r)	1.27 (r)	1.57 (r)
CorJet (data from [7])	Integral model	0.39 (r)	0.56 (r)	0.65 (r)	0.69 (r)	0.69 (r)
Yannopoulos and Bloutsos [69]	Integral model	1.12 (r)	1.70 (r)	2.12 (r)	2.27 (r)	1.78 (r)
Oliver et al. [67]	Integral model	0.46 (r)	0.74 (r)	1.12 (r)	1.61 (r)	2.32 (r)
Crowe et al. [68]	Integral model	0.53 (r)	0.88 (r)	1.22 (r)	1.50 (r)	1.63 (r)
Ramezani et al. [31]	RANS	–	0.71 (r)	0.82 (r)	–	–
Zhang et al. [28]	RANS	–	–	0.87	–	–

Denoted values by (r) are for the return point

*Two values were reported for LES: Before concentration build-up/On concentration build-up

**Two values were reported for LIF: Before concentration build-up/On concentration build-up

It is also worth noting that recent corrections in simple models which are based on integral methods exhibited that they could satisfactorily predict mean flow characteristics of negatively buoyant jets after the modification of the entrainment coefficient [64, 65] or the modification of the buoyancy flux conservation [21, 60, 66]. The comparisons made by Papakonstantis and Papanicolaou [65] for some common experiments [8, 12, 13, 58, 60] exhibited that the problem of underestimating flow parameters, i.e., geometrical characteristics and dilution, has been solved to some extent and the results of these simple models are closer to LES results.

5 Conclusions

Due to technological advances, these days, fresh water can be produced out of brackish and saline water by desalination plants. These plants take out the seawater inland and use various techniques to remove salt and other solutes from it. Desalination plants produce a concentrated effluent (brine) as a by-product that needs to be discharged back into the seas or oceans. Therefore, the main environmental impact of the desalination plants is attributed to the disposal of brine into the aquatic environment. The marine outfalls are developed to minimize these impacts by adequately diluting the brine in the sea. Due to its high density, the brine can simply reach the seafloor and rest on it. The high concentration of brine close to the bed is environmentally significant, as most of the impacts are subjected to less mobile benthic organisms and seagrasses. The inclined jets are a common way to dispose

of brine as they can clear the waste field from the source site and decrease its concentration to a great extent.

In the present study, the results of numerical (LES) and experimental (LIF) simulations on the discharge of dense jets at 15°, 30°, 45°, 60°, and 75° angles were presented. The results of each parameter were normalized and plotted along with the previously reported data. A table presented contains the previous data reported from experimental, analytical, and numerical investigations and quantitative comparisons made between them. Also, recent modifications that were reported for integral models on the estimation of mean flow characteristics of negatively buoyant jets were evaluated. It was found that LES and these modified models are close to the experimental observations even due that there are discrepancies between experimental data at the boundary, specifically.

A novel criterion was also proposed to guess when the flow reaches a quasi-steady-state. This is important in numerical simulations to reduce computational expenses, particularly for high-resolution and consequently high computational demanding approaches such as LES. The numerical model well estimated the trend of changes in flow trajectory and geometrical features; however, some discrepancies were observed compared to the experimental results. It was observed that dilutions were specifically underestimated up to 25%, which was found to be a common problem when comparing the results of numerical models with experimental data. However, large variations were observed in the experimental results of different scholars, which made comparisons unsure and difficult. It was observed that time-averaged dilution decreased along the centerline trajectory in a short distance as the bed was approached. Therefore, special attention was paid to dilution on the lower boundary. The reason for such discrepancy was found to be the concentration deposition near the stagnation region at the location of the impact point. This thin and more concentrated layer close to the bed is environmentally significant and may cause elevated exposures of the benthic organisms to high salinity levels, which could be fatal. In this work, we tried to shine a light on this complex problem to attract more attention to study boundary effects on brine flow features on the seafloor.

Acknowledgements The authors acknowledge the funding support of the Babol Noshirvani University of Technology through grant program No. BNUT/390035/1400.

Declarations

Conflict of interest The authors declare that they have no known competing financial interests or personal relationships that could have appeared to influence the work reported in this paper.

References

1. Abessi O (2018) Brine disposal and management—planning, design, and implementation. In: sustainable desalination handbook: plant selection, design and implementation
2. Saeedi M, Farahani AA, Abessi O, Bleninger T (2012) Laboratory studies defining flow regimes for negatively buoyant surface discharges into crossflow. *Environ Fluid Mech* 12:439–449. <https://doi.org/10.1007/S10652-012-9245-4>
3. Ghayoor S, Hamidi M, Abessi O (2019) Experimental analysis of turbulent flows in brine discharge of coastal desalination plants. *J Oceanogr* 10:101–111. <https://doi.org/10.29252/joc.10.39.101> (In Persian)
4. Roberts PJW, Ferrier A, Daviero G (1997) Mixing in inclined dense jets. *J Hydraul Eng* 123:693–699. [https://doi.org/10.1061/\(ASCE\)0733-9429\(1997\)123:8\(693\)](https://doi.org/10.1061/(ASCE)0733-9429(1997)123:8(693))

5. Abessi O, Roberts PJW (2017) Multiport diffusers for dense discharge in flowing ambient water. *J Hydraul Eng* 143:04017003. [https://doi.org/10.1061/\(ASCE\)HY.1943-7900.0001279](https://doi.org/10.1061/(ASCE)HY.1943-7900.0001279)
6. Kikkert GA, Davidson MJ, Nokes RI (2007) Inclined negatively buoyant discharges. *J Hydraul Eng* 133:545–554. [https://doi.org/10.1061/\(ASCE\)0733-9429\(2007\)133:5\(545\)](https://doi.org/10.1061/(ASCE)0733-9429(2007)133:5(545))
7. Jirka GH (2008) Improved discharge configurations for brine effluents from desalination plants. *J Hydraul Eng* 134:116–120. [https://doi.org/10.1061/\(ASCE\)0733-9429\(2008\)134:1\(116\)](https://doi.org/10.1061/(ASCE)0733-9429(2008)134:1(116))
8. Lai CCK, Lee JHW (2012) Mixing of inclined dense jets in stationary ambient. *J Hydro Environ Res* 6:9–28. <https://doi.org/10.1016/j.jher.2011.08.003>
9. Oliver CJ, Davidson MJ, Nokes RI (2013) Behavior of dense discharges beyond the return point. *J Hydraul Eng* 139:1304–1308. [https://doi.org/10.1061/\(ASCE\)HY.1943-7900.0000781](https://doi.org/10.1061/(ASCE)HY.1943-7900.0000781)
10. Cederwall K (1968) Hydraulics of marine waste water disposal. Chalmers tekniska högskola
11. Zeitoun MA, Reid RO, McHilheny WF, Mitchell TM (1970) Model studies of ocean outfall systems for desalination plants. Off Saline Water US Department of the Interior, Washington
12. Papakonstantis IG, Christodoulou GC, Papanicolaou PN (2011) Inclined negatively buoyant jets 1: geometrical characteristics. *J Hydraul Res*. <https://doi.org/10.1080/00221686.2010.537153>
13. Papakonstantis IG, Christodoulou GC, Papanicolaou PN (2011) Inclined negatively buoyant jets 2: concentration measurements. *J Hydraul Res*. <https://doi.org/10.1080/00221686.2010.542617>
14. Roberts PJW, Abessi O (2014) Optimization of desalination diffusers using three-dimensional laser-induced fluorescence. Rep Prep US Bur Reclam Agreeem
15. Antenucci JP, Ransome T, Ferguson M (2015) Field validation of a multiport brine diffuser in a coastal environment: implications for design. In: Australian Coasts and Ports 2015 Conference
16. Baum MJ, Albert S, Grinham A, Gibbs B (2019) Spatiotemporal influences of open-coastal forcing dynamics on a dense multiport diffuser outfall. *J Hydraul Eng* 145:05019004. [https://doi.org/10.1061/\(ASCE\)HY.1943-7900.0001622](https://doi.org/10.1061/(ASCE)HY.1943-7900.0001622)
17. Baum MJ, Gibbs B, Grinham A et al (2018) Near-field observations of an offshore multiport brine diffuser under various operating conditions. *J Hydraul Eng* 144:05018007. [https://doi.org/10.1061/\(ASCE\)HY.1943-7900.0001524](https://doi.org/10.1061/(ASCE)HY.1943-7900.0001524)
18. Abessi O, Roberts PJW (2014) Multiport diffusers for dense discharges. *J Hydraul Eng* 140:04014032. [https://doi.org/10.1061/\(ASCE\)HY.1943-7900.0000882](https://doi.org/10.1061/(ASCE)HY.1943-7900.0000882)
19. Papakonstantis IG, Tsatsara EI (2018) Trajectory characteristics of inclined turbulent dense jets. *Environ Process* 5:539–554. <https://doi.org/10.1007/s40710-018-0307-6>
20. Papakonstantis IG, Tsatsara EI (2019) Mixing characteristics of inclined turbulent dense jets. *Environ Process*. <https://doi.org/10.1007/s40710-019-00359-w>
21. Crowe AT, Davidson MJ, Nokes RI (2016) Velocity measurements in inclined negatively buoyant jets. *Environ Fluid Mech* 16:503–520. <https://doi.org/10.1007/s10652-015-9435-y>
22. Ramakanth A, Davidson MJ, Nokes RI (2022) Laboratory study to quantify lower boundary influences on desalination discharges. *Desalination* 529:115641. <https://doi.org/10.1016/J.DESAL.2022.115641>
23. Vafeiadou P, Papakonstantis I, Christodoulou G (2005) Numerical simulation of inclined negatively buoyant jets. In: The 9th international conference on environmental science and technology, September. pp 1–3
24. Oliver CJ, Davidson MJ, Nokes RI (2008) k- ϵ Predictions of the initial mixing of desalination discharges. *Environ Fluid Mech* 8:617–625. <https://doi.org/10.1007/s10652-008-9108-1>
25. Jirka GH (2004) Integral model for turbulent buoyant jets in unbounded stratified flows. Part I: single round jet. *Environ Fluid Mech* 4:1–56. <https://doi.org/10.1023/A:1025583110842>
26. Lee JHW, Cheung V, Wang WP, Cheung SKB (2000) Lagrangian modeling and visualization of rosette outfall plumes. In: Proc Hydroinformatics Iowa
27. Kheirkhah Gildeh H, Mohammadian A, Nistor I, Qiblawey H (2015) Numerical modeling of 30° and 45° inclined dense turbulent jets in stationary ambient. *Environ Fluid Mech* 15:537–562. <https://doi.org/10.1007/s10652-014-9372-1>
28. Zhang S, Law AW-K, Jiang M (2017) Large eddy simulations of 45° and 60° inclined dense jets with bottom impact. *J Hydro Environ Res* 15:54–66. <https://doi.org/10.1016/j.jher.2017.02.001>
29. Abessi O, Roberts PJW (2015) Effect of nozzle orientation on dense jets in stagnant environments. *J Hydraul Eng* 141:06015009. [https://doi.org/10.1061/\(ASCE\)HY.1943-7900.0001032](https://doi.org/10.1061/(ASCE)HY.1943-7900.0001032)
30. Tahmooresi S, Ahmadyar D (2021) Effects of turbulent Schmidt number on CFD simulation of 45° inclined negatively buoyant jets. *Environ Fluid Mech* 21:39–62. <https://doi.org/10.1007/s10652-020-09762-6>
31. Ramezani M, Abessi O, Firoozjaee AR (2021) Effect of proximity to bed on 30° and 45° inclined dense jets: a numerical study. *Environ Process* 8:1141–1164. <https://doi.org/10.1007/s40710-021-00533-z>
32. Pope SB (2000) Turbulent flows. Cambridge University Press

33. Liu X, Zhang J (2019) Computational fluid dynamics: applications in water, wastewater, and storm-water treatment. American Society of Civil Engineers, Reston
34. Zhang S, Jiang B, Law AW-K, Zhao B (2016) Large eddy simulations of 45° inclined dense jets. *Environ Fluid Mech* 16:101–121. <https://doi.org/10.1007/s10652-015-9415-2>
35. Tofighian H, Amani E, Saffar-Avval M (2020) A large eddy simulation study of cyclones: the effect of sub-models on efficiency and erosion prediction. *Powder Technol* 360:1237–1252. <https://doi.org/10.1016/j.powtec.2019.10.091>
36. Kim W-W, Menon S (1995) A new dynamic one-equation subgrid-scale model for large eddy simulations. In: 33rd Aerospace Sciences Meeting and Exhibit. American Institute of Aeronautics and Astronautics, Reston, Virginia
37. Holzmann T (2018) Mathematics, numerics, derivations and OpenFOAM®. Holzmann CFD
38. Jasak H (1996) Error analysis and estimation for the finite volume method with applications to fluid flows. Imperial College London University of London
39. Martínez J, Piscaglia F, Montorfano A, Onorati A, Aithal SM (2015) Influence of spatial discretization schemes on accuracy of explicit LES: canonical problems to engine-like geometries. *Comput Fluids* 117:62–78. <https://doi.org/10.1016/j.compfluid.2015.05.007>
40. Epikhin AS (2019) Numerical schemes and hybrid approach for the simulation of unsteady turbulent flows. *Math Model Comput Simul* 11:1019–1031. <https://doi.org/10.1134/S2070048219060024>
41. Moukalled F, Mangani L, Darwish M (2016) The finite volume method in computational fluid dynamics. Springer International Publishing
42. Celik IB, Cehreli ZN, Yavuz I (2005) Index of resolution quality for large eddy simulations. *J Fluids Eng* 127:949–958. <https://doi.org/10.1115/1.1990201>
43. Pope SB (2004) Ten questions concerning the large-eddy simulation of turbulent flows. *New J Phys* 6:1–35. <https://doi.org/10.1088/1367-2630/6/1/035>
44. Greenshields CJ (2015) OpenFoam user guide. OpenFOAM Foundation Ltd
45. Tian X, Roberts PJW (2003) A 3D LIF system for turbulent buoyant jet flows. *Exp Fluids* 35:636–647. <https://doi.org/10.1007/s00348-003-0714-x>
46. Abessi O, Ramani Firoozjaye A, Hamidi M, Bassam M, Khodabakhshi Z (2020) Three dimensional laser scanning system for illumination of fluorescent flow for the environmental hydraulics investigations. *J Hydraul* 14:69–81. <https://doi.org/10.30482/JHYD.2020.105499> (in Persian)
47. Daviero GJ, Roberts PJW, Maile K (2001) Refractive index matching in large-scale stratified experiments. *Exp Fluids* 31:119–126. <https://doi.org/10.1007/s003480000260>
48. Gungor E, Roberts PJW (2009) Experimental studies on vertical dense jets in a flowing current. *J Hydraul Eng* 135:935–948. [https://doi.org/10.1061/\(ASCE\)HY.1943-7900.0000106](https://doi.org/10.1061/(ASCE)HY.1943-7900.0000106)
49. Fedele F, Abessi O, Roberts PJ (2015) Symmetry reduction of turbulent pipe flows. *J Fluid Mech* 779:390–410. <https://doi.org/10.1017/jfm.2015.423>
50. Fischer HB, List JE, Koh CR, Imberger J, Brooks N (1979) Mixing in inland and coastal waters. Elsevier
51. Roberts PJW, Toms G (1987) Inclined dense jets in flowing current. *J Hydraul Eng* 113:323–340. [https://doi.org/10.1061/\(ASCE\)0733-9429\(1987\)113:3\(323\)](https://doi.org/10.1061/(ASCE)0733-9429(1987)113:3(323))
52. Abessi O, Roberts PJW (2016) Dense jet discharges in shallow water. *J Hydraul Eng* 142:04015033. [https://doi.org/10.1061/\(ASCE\)HY.1943-7900.0001057](https://doi.org/10.1061/(ASCE)HY.1943-7900.0001057)
53. Jiang B, Law AW-K, Lee JH-W (2014) Mixing of 30° and 45° inclined dense jets in shallow coastal waters. *J Hydraul Eng* 140:241–253. [https://doi.org/10.1061/\(ASCE\)HY.1943-7900.0000819](https://doi.org/10.1061/(ASCE)HY.1943-7900.0000819)
54. Shao D, Law AWK (2010) Mixing and boundary interactions of 30° and 45° inclined dense jets. *Environ Fluid Mech* 10:521–553. <https://doi.org/10.1007/s10652-010-9171-2>
55. Ramezani M, Abessi O, Rahmani Firoozjaye A (2021) Experimental study of geometrical characteristics of free and boundary-affected 30° inclined dense jets in unstratified stagnant environments. *J Water Wastewater* 32:91–102. <https://doi.org/10.22093/WWJ.2020.238900.3047> (in Persian)
56. Aghajanpour A (2018) Experimental and numerical modeling of upwardly inclined turbulent dense jet unjection into a stagnant ambient. Babol Noshirvani University of Technology
57. Crowe AT (2013) Inclined negatively buoyant jets and boundary interaction. University of Canterbury
58. Kikkert GA (2006) Buoyant jets with two and three-dimensional trajectories. University of Canterbury
59. Cipollina A, Brucato A, Grisafi F, Nicosia S (2005) Bench-scale investigation of inclined dense jets. *J Hydraul Eng* 131:1017–1022. [https://doi.org/10.1061/\(ASCE\)0733-9429\(2005\)131:11\(1017\)](https://doi.org/10.1061/(ASCE)0733-9429(2005)131:11(1017))
60. Oliver CJ, Davidson MJ, Nokes RI (2013) Removing the boundary influence on negatively buoyant jets. *Environ Fluid Mech*. <https://doi.org/10.1007/s10652-013-9278-3>
61. Reungoat D, Rivière N, Fauré JP (2007) 3C PIV and PLIF measurement in turbulent mixing. *J Vis* 10:99–110. <https://doi.org/10.1007/BF03181809>

62. Ramezani M, Abessi O, Rahmani Firoozjaye A (2020) Numerical simulation of dense discharges from 30° submerged inclined jet in free and bed-affected conditions. *J Hydraul* 15:75–91. <https://doi.org/10.30482/JHYD.2020.228141.1454> (in Persian)
63. Baum MJ, Gibbes B (2020) Field-scale numerical modeling of a dense multiport diffuser outfall in crossflow. *J Hydraul Eng* 146:05019006. [https://doi.org/10.1061/\(ASCE\)HY.1943-7900.0001635](https://doi.org/10.1061/(ASCE)HY.1943-7900.0001635)
64. Papanicolaou PN, Papakonstantis IG, Christodoulou GC (2008) On the entrainment coefficient in negatively buoyant jets. *J Fluid Mech* 614:447–470. <https://doi.org/10.1017/S0022112008003509>
65. Papakonstantis IG, Papanicolaou PN (2022) On the computational modeling of inclined brine discharges. *Fluids* 7:86. <https://doi.org/10.3390/FLUIDS7020086>
66. Bloutsos AA, Yannopoulos PC (2020) Revisiting mean flow and mixing properties of negatively round buoyant jets using the escaping mass approach (EMA). *Fluids* 5:131. <https://doi.org/10.3390/FLUIDS5030131>
67. Oliver CJ, Davidson MJ, Nokes RI (2013) Predicting the near-field mixing of desalination discharges in a stationary environment. *Desalination* 309:148–155. <https://doi.org/10.1016/J.DESAL.2012.09.031>
68. Crowe AT, Davidson MJ, Nokes RI (2016) Modified reduced buoyancy flux model for desalination discharges. *Desalination* 378:53–59. <https://doi.org/10.1016/J.DESAL.2015.08.010>
69. Yannopoulos PC, Bloutsos AA (2012) Escaping mass approach for inclined plane and round buoyant jets. *J Fluid Mech* 695:81–111. <https://doi.org/10.1017/JFM.2011.564>

Publisher's Note Springer Nature remains neutral with regard to jurisdictional claims in published maps and institutional affiliations.